A&A 542, A109 (2012)
DOI: 10.1051/0004-6361/201219093

Astronomy & Astrophysics

Discovery of the neutron star spin and a possible orbital period from the Be/X-ray binary IGR J05414-6858 in the LMC⋆

R. Sturm[1], F. Haberl[1], A. Rau[1], E. S. Bartlett[2], X.-L. Zhang[1], P. Schady[1], W. Pietsch[1], J. Greiner[1], M. J. Coe[2], and A. Udalski[3]

[1] Max-Planck-Institut für extraterrestrische Physik, Giessenbachstraße, 85748 Garching, Germany
e-mail: rsturm@mpe.mpg.de
[2] School of Physics and Astronomy, University of Southampton, Highfield, Southampton SO17 1BJ, UK
[3] Warsaw University Observatory, Aleje Ujazdowskie 4, 00-478 Warsaw, Poland

Received 22 February 2012 / Accepted 29 April 2012

ABSTRACT

Context. The number of known Be/X-ray binaries in the Large Magellanic Cloud is small compared to the observed population of the Galaxy or the Small Magellanic Cloud. The discovery of a system in outburst provides the rare opportunity to measure its X-ray properties in detail.
Aims. IGR J05414-6858 was discovered in 2010 with INTEGRAL and was found in another outburst with the *Swift* satellite in 2011. To characterise the system, we analysed the data from a follow-up *XMM-Newton* target of opportunity observation of the 2011 outburst and investigated the stellar counterpart with photometry and spectroscopy.
Methods. We modelled the X-ray spectra from the EPIC instruments on *XMM-Newton* and compared them with *Swift* archival data. We searched for periodicities and variability in the X-ray and optical light curves. The optical counterpart was classified using spectroscopy obtained with ESO's Faint Object Spectrograph at NTT.
Results. The X-ray spectra as seen in 2011 are relatively hard with a photon index of ∼0.3−0.4 and show only low absorption. They deviate significantly from earlier spectra of a probable type-II outburst in 2010. The neutron star spin period of $P_{\rm spin}$ = 4.4208 s was discovered with EPIC-pn. The *I*-band light curve revealed a transition from a low to a high state around MJD 54 500. The optical counterpart is classified as B0-1 IIIe and shows Hα emission and a variable near-infrared excess that vanishes during the 2010 outburst. In the optical high state, we found a periodicity at 19.9 days, probably caused by binarity and indicating the orbital period.

Key words. galaxies: individual: Large Magellanic Cloud – stars: emission-line, Be – stars: neutron – X-rays: binaries

1. Introduction

Depending on the donor star, high-mass X-ray binaries (HMXBs) are divided into super-giant systems and Be/X-ray binaries (BeXRBs, e.g. Reig 2011). In the latter case, a poorly understood mechanism causes matter ejection of the Be star in the equatorial plane, leading to the build-up of an equatorial decretion disc around the Be star (Okazaki 2001). This disc dominates the emission of the system in infrared and in some emission lines such as Hα. The variability of this emission points to the instability of these discs. Owing to a supernova kick, a neutron star (NS) can have an eccentric orbit around the Be star. During periastron passage the NS can accrete matter from the decretion disc, causing a so-called type-I X-ray outburst, which lasts for several days at typical luminosities of 10^{36} erg s^{-1}. During disc instabilities, the NS can accrete a large part of the decretion disc, resulting in type-II outbursts with luminosities of up to 10^{37} erg s^{-1} for several weeks.

The transient behaviour of Be/X-ray binaries and the wide extent of the Large Magellanic Cloud (LMC) on the sky, which imposes a low observational coverage by X-ray missions, complicate the discovery and investigation of Be/X-ray binaries in this galaxy. In contrast to that, the Small Magellanic Cloud (SMC) was monitored with RXTE for about 14 years (Galache et al. 2008). Therefore, only nine HMXB X-ray pulsars are known to date in the LMC, which inhibits a statistical comparison of this sample with those of the Galaxy and the SMC. In the Galaxy and the SMC ∼66 and ∼55 HMXB pulsars are known, respectively. A major fraction of the pulsars is found in Be/X-ray binaries (e.g. Coe et al. 2010). Population studies of these systems are important for understanding the stellar evolution, because they allow one to estimate e.g. supernova kick velocities (Coe 2005) or the star formation history (Antoniou et al. 2010; Mineo et al. 2011). Recently, a bimodal NS spin period distribution for the Galactic and SMC samples has been associated with two different types of supernovae (Knigge et al. 2011). To enable these statistical studies for the LMC, it is necessary to successively build up a larger sample of X-ray measurements of pulsars in outburst.

In 2010, IGR J05414-6858 was discovered serendipitously within INTEGRAL observations of SN 1987A (Grebenev & Lutovinov 2010) and was later localised (Lutovinov & Grebenev 2010) and identified as Be-X-ray binary (Rau et al. 2010) with *Swift* and GROND follow-up observations. In 2011, *Swift* performed an ultraviolet (UV) survey of the LMC (PI: S. Immler). This provided a shallow coverage of this galaxy with the *Swift* X-ray telescope (XRT) and allowed the detection of bright X-ray transients. In an observation on 2011 Aug. 5 an outburst of IGR J05414-6858 was detected (Sturm et al. 2011b), which

⋆ Based on observations with *XMM-Newton*, an ESA Science Mission with instruments and contributions directly funded by ESA Member states and the USA (NASA).

Table 1. X-ray observations of IGR J05414-6858.

Observation	ObsID	Date	Time (UT)	Instrument	Mode[a]	Offax[b] [′]	Net Exp [ks]	Net Cts[c]	R_{sc}[d] [″]
XMM 2001	0094410101	2001-10-19	17:49–20:30	EPIC-pn	ff-medium	8.2	8.2	<26	30
			17:09–20:29	EPIC-MOS1	ff-medium	7.2	11.7	<5	30
			17:09–20:29	EPIC-MOS2	ff-medium	6.9	11.7	<14	30
XMM 2011	0679380101	2011-08-13	07:45–14:07	EPIC-pn	ff-thin	1.1	7.2	2018	21
			07:22–14:07	EPIC-MOS1	ff-medium	1.2	9.4	863	29
			07:22–14:07	EPIC-MOS2	ff-medium	1.2	9.4	954	31
Swift 2010a	00031745001	2010-06-25	05:35–09:10	XRT	pc	5.3	3.9	221	40
Swift 2010b	00031745002	2010-06-30	01:14–23:59	XRT	pc	2.0	5.2	497	50
Swift 2011a	00045428001	2011-08-05	15:28–22:26	XRT	pc	10.5	3.3	40	40
Swift 2011b	00031745003	2011-08-09	23:53–04:55	XRT	pc	1.8	3.7	120	40
Swift 2011c	00031745004	2011-08-12	00:03–22:53	XRT	pc	2.4	4.1	100	40
Swift 2011d	00031745005	2011-08-20	00:25–16:53	XRT	pc	3.1	2.1	<6	40
Swift 2011e	00031745006	2011-08-24	02:44–04:29	XRT	pc	2.5	1.2	<5	40

Notes. [(a)] Observation setup: full-frame mode (ff) and photon-counting mode (pc). For *XMM-Newton*, the filter is given as well. [(b)] Off-axis angle under which the source was observed. [(c)] Net counts as used for spectral analysis in the (0.2−10.0) keV band for *XMM-Newton* and in the (0.3−6.0) keV band for *Swift*. [(d)] Radius of the circular source extraction region.

allowed us to request an *XMM-Newton* target of opportunity (ToO) observation.

In this study, we report our analysis of the *XMM-Newton* observation of IGR J05414-6858. The detection of the NS spin period adds the tenth X-ray pulsar in the LMC sample and a detailed X-ray spectral and temporal analysis allows a characterisation of the system. We compare our new results to those from archival *Swift* data and discuss complementary optical data to characterise the optical counterpart and the circumstellar disc.

2. Observations and data reduction

2.1. XMM-Newton

The *XMM-Newton* (Jansen et al. 2001) ToO observation was performed on 2011 Aug. 13. The source was observed on-axis, placed on CCD4 of EPIC-pn (Strüder et al. 2001) and CCD1 of both EPIC-MOS (Turner et al. 2001) detectors. We used *XMM-Newton* SAS 11.0.0[1] to process the data. Unfortunately, the observation was affected by an increased background caused by soft protons. During the first ∼11.5 ks of the ∼17 ks observation, the background was at a moderately elevated level, allowing the selection of time intervals where the background rate in the (7.0−15.0) keV band was below 50 cts ks^{-1} arcmin^{-2} for EPIC-pn and below 4 cts ks^{-1} arcmin^{-2} for EPIC-MOS. The detailed observation setup is recorded in Table 1. Here, we also list an *XMM-Newton* observation from 2001 that covers the position of IGR J05414-6858, in which the source was not detected. We used this observation to derive an upper limit for the flux. For EPIC-pn, we used single- and double-pixel events and single- to quadruple-pixel events in the case of EPIC-MOS, all having `FLAG = 0`. Background events were selected from a point-source-free area on the same CCDs as the source. Source events were extracted from a circle, with radius optimised for the signal-to-noise ratio by the SAS task `eregionanalyse`. We created spectra and response matrices with `especget` and used a binning to have at least a signal to noise ratio of 5 for each bin. For time series, the photon arrival times were randomised within the CCD frame time and calculated for the solar system barycentre.

2.2. Swift

We re-analysed archival *Swift*/XRT observations. The spectra were created by using the `ftool`[2] `xselect` to select events in the cleaned level-3 event files within a circle, placed on the source with radii given in Table 1. Background spectra were created from a circular extraction region with radius of 200″. The spectra were binned to have ≥20 cts bin^{-1}. The ancillary response files were calculated with `xrtmkarf`. *Swift* observations of IGR J05414-6858 including non-detections, are also listed in Table 1.

2.3. NIR, optical, and UV photometry

Optical photometry of IGR J05414–6858 was obtained with OGLE, GROND and *Swift*/UVOT. The optical counterpart was monitored regularly during the Optical Gravitational Lensing Experiment (OGLE) of phase III (Udalski et al. 2008) between October 2001 and April 2009 in the *I*-band. The source identification is OGLEIII LMC175.4.21714.

The Gamma-Ray burst Optical Near-ir Detector (GROND; Greiner et al. 2008) at the MPG/ESO 2.2 m telescope in La Silla, Chile, observed the source at three epochs in June 2010 and January 2012. Preliminary results of the 2010 observations were already presented in Rau et al. (2010). GROND is a seven-channel imager that observes in four optical and three near-IR channels simultaneously. The IGR J05414–6858 data were reduced and analysed with the standard tools and methods described in Krühler et al. (2008). The photometry was obtained using point-spread-function (PSF) fitting taking into account the contamination from the two nearby sources (see Fig. 1). Calibration was performed against observations of an SDSS standard star field ($g'r'i'z'$) or against selected 2MASS stars (Skrutskie et al. 2006) (JHK_S). This resulted in 1σ accuracies of 0.04 mag ($g'z'$), 0.03 mag ($r'i'$), 0.05 mag (JH), and 0.07 mag (K_S).

[1] Science Analysis Software (SAS), http://xmm.esac.esa.int/sas/

[2] http://heasarc.nasa.gov/ftools/

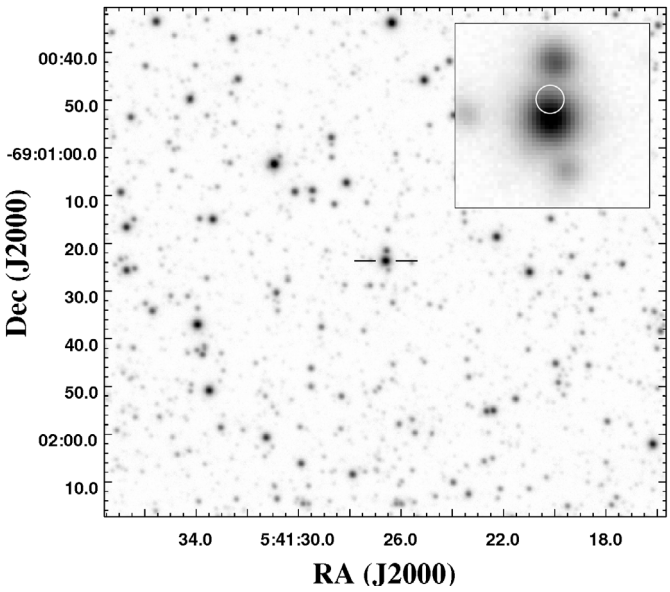

Fig. 1. GROND r'-band finding chart. Lines mark the counterpart of IGR J05414-6858. In the zoom-in, the *XMM-Newton* position is marked with a white circle with radius of the 1σ position uncertainty of 0.52″. The astrometric solution accuracy of the GROND image is 0.47″ in RA and 0.21″ in Dec.

The Ultraviolet/Optical Telescope (UVOT) onboard *Swift* has three optical (v b u) and three UV filters ($uvw1$ $uvm2$ $uvw2$). IGR J05414-6858 was observed in all UVOT filters during the pointed X-ray observations. For the LMC UV-survey observation 00045428001, the source is not in the field of view of the UVOT. Photometry was carried out on pipeline-processed sky images downloaded from the *Swift* data centre[3], following the standard UVOT procedure (Poole et al. 2008).

2.4. Optical spectroscopy

Optical spectroscopy was taken with the ESO Faint Object Spectrograph (EFOSC2) mounted at the Nasmyth B focus of the 3.6 m New Technology Telescope (NTT), La Silla, Chile on the nights of 2011 December 8 and 10. The EFOSC2 detector (CCD#40) is a Loral/Lesser, Thinned, AR coated, UV flooded, MPP chip with 2048 × 2048 pixels corresponding to 4.1′ × 4.1′ on the sky. The instrument was in longslit mode with a slit width of 1.5″. Grisms 14 and 20 were used for blue and red end spectroscopy, respectively. Grism 14 has a wavelength range of $\lambda\lambda$3095−5085 Å and a grating of 600 lines mm^{-1} and a dispersion of 1 Å pixel^{-1}. The resulting spectra have a spectral resolution of ∼12 Å. Grism 20 is one of the two new volume-phase holographic grisms recently added to EFOSC2. It has a shorter wavelength range, from 6047−7147 Å, but a superior dispersion of 0.55 Å pixel^{-1} and 1070 lines mm^{-1}. This produced a spectral resolution for our red end spectra of ∼6 Å. Filter OG530 was used to block second-order effects. The data were reduced using the standard packages available in the Image Reduction and Analysis Facility IRAF. Wavelength calibration was implemented using comparison spectra of helium and argon lamps taken throughout the observing run with the same instrument configuration. The spectra were normalised to remove the continuum and a redshift correction was applied corresponding to the recession velocity of the LMC (−280 km s^{-1}, Paturel et al. 2002).

[3] http://www.swift.ac.uk/swift_portal

3. Analyses and results of X-ray data

3.1. X-ray coordinates

We created X-ray images from all three EPIC cameras in the *XMM-Newton* standard energy sub-bands. A simultaneous source detection was performed on these images with `edetect_chain`. The best-fit source position is RA (J2000) = $05^{h}41^{m}26\overset{s}{.}62$ and Dec (J2000) = −69°01′23.″0. The 1σ uncertainty of the position is 0.52″, where we assumed a systematic error of 0.5″, which is quadratically added to the statistical error. The angular separation to the optical counterpart is 0.52″ for the 2MASS position and 0.69″ for the GROND position (star A, Rau et al. 2010). The distance to the *Swift* position of Lutovinov & Grebenev (2010) is 2.0″ with an uncertainty in the *Swift* measurement of ∼3″. A finding chart obtained from GROND data is presented in Fig. 1. The white circle in the zoom-in gives the *XMM-Newton* position. The improved X-ray coordinates from the *XMM-Newton* observation additionally confirm the identification of the X-ray source with the optical counterpart.

3.2. Spectral analysis

Spectral analysis was performed with `xspec` (Arnaud 1996) version 12.7.0. The three *XMM-Newton* EPIC spectra were fitted simultaneously and we included constant factors in the models to consider instrumental differences. For all models, we obtained consistent values of $C_{\rm MOS1}$ = 1.11 ± 0.08 and $C_{\rm MOS2}$ = 1.10 ± 0.08 relative to EPIC-pn ($C_{\rm pn}$ = 1). Therefore, the fluxes for all instruments are consistent within uncertainties, because EPIC-MOS is known to derive ∼5% higher values compared to EPIC-pn. All other model parameters were forced to be the same for all instruments. The spectra are well described by an absorbed power-law. The photoelectric absorption was modelled by a fixed Galactic foreground column density of $N_{\rm H,Gal}$ = 6 × 10^{20} cm^{-2} (Dickey & Lockman 1990) with abundances according to Wilms et al. (2000). An additional column density $N_{\rm H,LMC}$ was determined in the fit. It accounts for the interstellar medium of the LMC and source intrinsic absorption and the abundances were set to 0.5 for elements heavier than helium (Russell & Dopita 1992).

We furthermore tested the spectra for the existence of typical features of BeXRBs. A possible soft excess (e.g. Eger & Haberl 2008; Hickox et al. 2004) was modelled by a black-body (Model: PL+BB) or a multi-temperature disc black-body model (PL+DiscBB). The additional model component improves the fit only marginally, but demonstrates model-dependent uncertainties for the power-law parameters. The f-test probability for these additional components is about 13%. We used the black-body model to derive an upper limit for a soft-component contribution. A soft excess can account only for <1% of the detected flux and up to 22.0% of the unabsorbed luminosity in the (0.2−10.0) keV band. The derived radius of the emission region from the black-body is too large for an NS. With the disc model we obtain a similar inner radius for an inclination of Θ = 0 ($R_{\rm in} \propto (\cos\Theta)^{-1/2}$). Also according to Hickox et al. (2004), we obtain an inner disc radius of $R_{\rm in} = (L_{\rm X}/4\pi\sigma T^4)^{1/2}$ = 52 km. Fluorescent iron line emission at 6.4 keV was modelled with a Gaussian line, with a fixed central energy and no measurable broadening. Here we also receive only a marginal improvement of the fit and a line

Table 2. Spectral fit results.

Observation	Model[a]	$N_{H,LMC}$ [10^{21} cm^{-2}]	Γ	kT [eV]	R^b [km]	EW_{Fe} [eV]	Flux[c] [10^{-12} erg cm^{-2} s^{-1}]	$L_x{}^d$ [10^{36} erg s^{-1}]	χ^2_{red}	d.o.f.
XMM 2011	PL	<0.89	$0.32^{+0.03}_{-0.05}$	–	–	–	$3.01^{+0.24}_{-0.32}$	0.91	0.92	118
	PL+BB	$4.98^{+3.4}_{-3.8}$	$0.40^{+0.07}_{-0.09}$	112^{+56}_{-23}	62^{+66}_{-46}	–	$2.98^{+0.20}_{-0.35}$	0.98	0.91	116
	PL+BB+Fe	$4.98^{+3.6}_{-3.6}$	$0.41^{+0.07}_{-0.09}$	111^{+49}_{-23}	62^{+73}_{-45}	78^{+71}_{-70}	$2.97^{+0.37}_{-0.47}$	0.98	0.88	115
	PL+DiscBB	$3.68^{+2.6}_{-1.4}$	$0.39^{+0.08}_{-0.08}$	128^{+85}_{-33}	49^{+134}_{-44}	–	$2.98^{+0.16}_{-0.33}$	1.01	0.91	116
Swift 2010a	PL	$1.9^{+2.0}_{-1.4}$	$0.78^{+0.18}_{-0.17}$	–	–	–	$5.6^{+1.1}_{-1.6}$	1.77	1.03	31
Swift 2010b							$9.2^{+1.3}_{-1.9}$	2.91		
Swift 2011a	PL	<2.6	$0.25^{+0.14}_{-0.22}$	–	–	–	$5.4^{+2.6}_{-5.4}$	1.62	1.18	8
Swift 2011b							$5.1^{+1.3}_{-4.5}$	1.51		
Swift 2011c							$3.5^{+9.8}_{-3.1}$	1.04		

Notes. [a] For definition of spectral models see text. [b] Radius of the emitting area (for BB) or inner disc radius for an inclination of $\Theta = 0$ (for DiscBB, for the definition see text). [c] Observed flux in the (0.2−10.0) keV band, derived by integrating the best-fit model. [d] Source intrinsic X-ray luminosity in the (0.2−10.0) keV band corrected for absorption and assuming a distance of the source of 50 kpc.

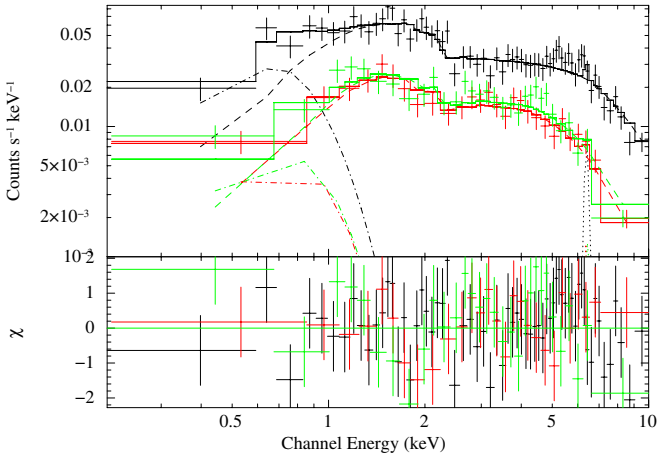

Fig. 2. EPIC-pn (black), EPIC-MOS1 (red), EPIC-MOS2 (green) spectra, together with the best-fit po+bb+Fe model (solid line) and its individual components: power-law (dashed), black-body (dashed-dotted) and Fe line (dotted). *The lower panel* shows the residuals.

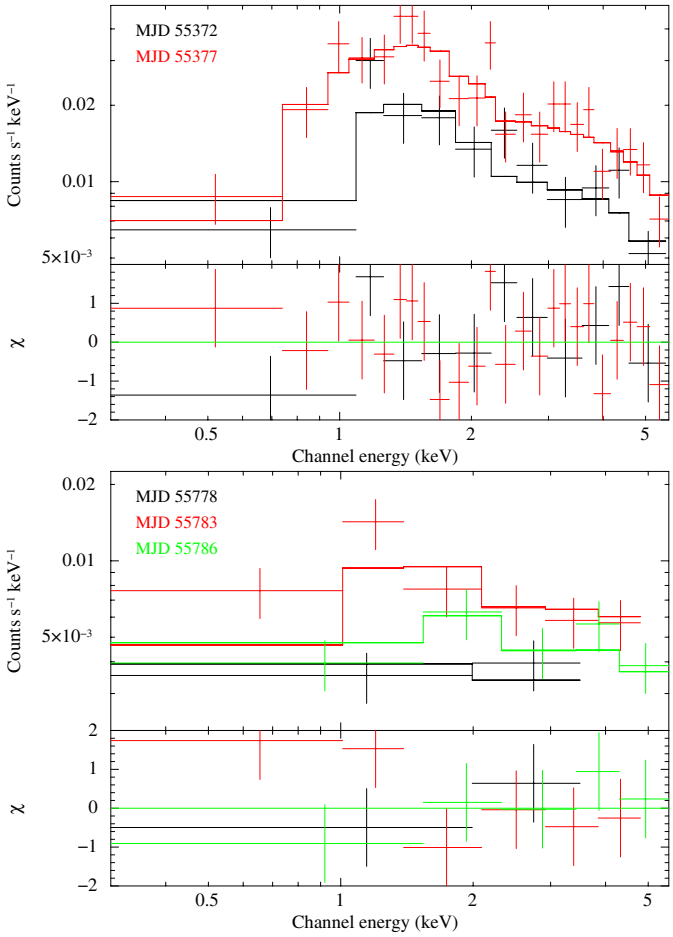

Fig. 3. *Swift* spectra of IGR J05414-6858 from 2010 (*top*) and 2011 (*bottom*) with best-fit power-law model. *Lower panels* give the residuals.

flux of $2.8 \pm 2.6 \times 10^{-6}$ photons cm^{-2} s^{-1}. The spectrum and best-fit model are presented in Fig. 2 and the best-fit results are listed in Table 2. All uncertainties and limits correspond to a 90% confidence level ($\Delta\chi^2 = 2.71$).

To investigate the spectral variability, we compared the EPIC spectra to the archival *Swift* spectra. The lower statistics only allowed us to fit the power-law model. For the two spectra in 2010, $N_{H,LMC}$ and Γ are consistent within errors. No significant evolution was found in the three *Swift* spectra of 2011. We assumed that the spectral shape is time-independent during the individual outbursts, and fitted the model simultaneously to the two 2010 and three 2011 *Swift* spectra (see Fig. 3). The fluxes were individually determined for all observations. The results are also listed in Table 2. There is significant spectral variability observed between the outbursts of IGR J05414-6858 in 2010 and 2011, where the recent outburst exhibits a harder X-ray spectrum, consistent with the *XMM-Newton* 2011 observation. If we fit the *Swift* 2010 data with the spectral model derived from the *XMM-Newton* 2011 observation (allowing a re-normalisation), the fit degrades from $\chi^2_{red} = 1.03$ to 1.75. In contrast to that, the χ^2_{red} improves from 1.18 to 1.06 ($\chi^2 = 10.6$, d.o.f. = 10), if we fit the *Swift* 2011 spectra with the *XMM-Newton*-derived model. This is caused by the increase of the degrees of freedom.

Because the lower photon index in 2011 is seen with *XMM-Newton* and *Swift*, this is unlikely to be caused by the

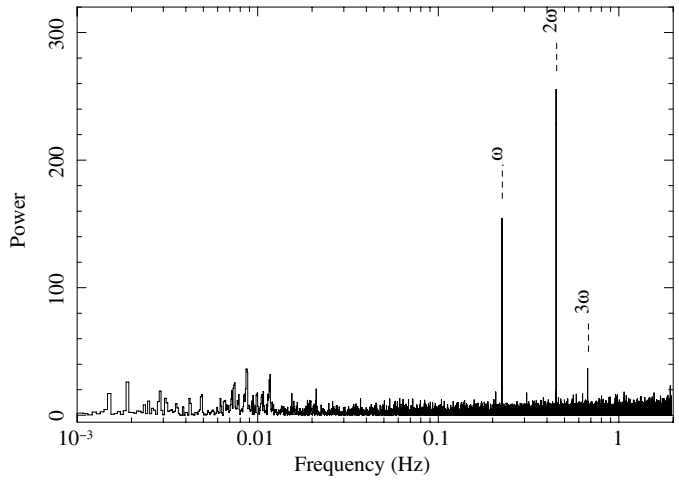

Fig. 4. Power density spectrum of IGR J05414-6858 for the EPIC-pn time series in the (0.2−10.0) keV band. The best-fit frequency of $\omega = 0.2262$ Hz and its first and second harmonics are marked with dashed lines.

high background during the *XMM-Newton* observation or by instrumental differences.

3.3. Pulsations

A strong signal at $\omega = 0.2262$ Hz and its first harmonic appeared in a fast Fourier transformation (FFT) of the EPIC-pn time series in the (0.2−10.0) keV band. The power density spectrum is plotted in Fig. 4. The signal is also clearly present in the (0.2−2.0) keV and (2.0−10.0) keV sub-bands. The period is not resolved by EPIC-MOS (2.6 s frame time), because the period is shorter than twice the frame time of the instrument, i.e. ω is above the Nyquist frequency. The same holds for the *Swift* data (2.5 s frame time). A χ^2 test, a Bayesian odds ratio (Gregory & Loredo 1996), and a Rayleigh Z^2 test for one harmonic (Haberl & Zavlin 2002; Buccheri et al. 1983) around the periodicity signal are shown in Fig. 5. All tests independently confirm the pulse period. Following Haberl et al. (2008), we used the Bayesian detection method to determine the pulse period and a 1σ uncertainty of 4.420866(2) s on 2011-08-13.

Figure 6 shows the folded background-subtracted light curves from EPIC-pn in the total (0.2−10.0) keV band and the standard sub-bands (0.2−0.5) keV, (0.5−1.0) keV, (1.0−2.0) keV, (2.0−4.5) keV, and (4.5−10.0) keV, where we merged the first two bands to increase the statistics. Hardness-ratio (HR) variations are also presented. The HRs are defined by $\mathrm{HR}_i = (R_{i+1} - R_i)/(R_{i+1} + R_i)$ with R_i denoting the background-subtracted count rate in the standard energy band i (with i from 1 to 4). In the light curves, two narrow peaks are seen within one period having only small variations in energy. By modelling the (0.2−10.0) keV curve with a non-pulsating contribution and one Gaussian for each peak, we estimate a pulsed fraction of (48 ± 7)% in the total flux, and a flux ratio for both peaks of 2.3 ± 0.5.

A search for pulsations in the INTEGRAL ISGRI observations of 2010 was performed. We detect the source at 0.28 ± 0.04 cts s^{-1} in the (20−40) keV band, but could not find a significant period in the power density spectrum or variability in the 4.4208 s folded light curve. This might be caused by binary orbital modulations, because the INTEGRAL observations cover a long time.

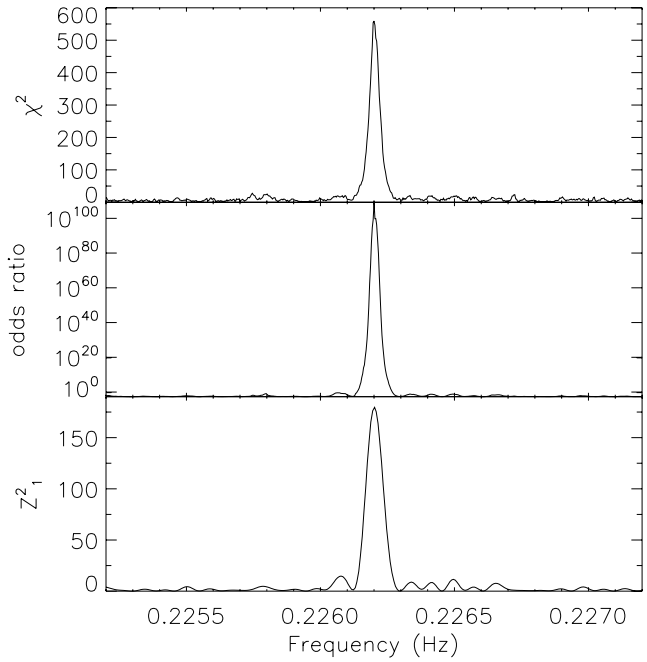

Fig. 5. *Top*: χ^2 test for persistence of the EPIC-pn light curve, around trial frequencies between 0.2252 and 0.2272 Hz. *Middle*: frequency dependence of the Bayesian odds ratio. *Bottom*: Rayleigh Z_1^2 test.

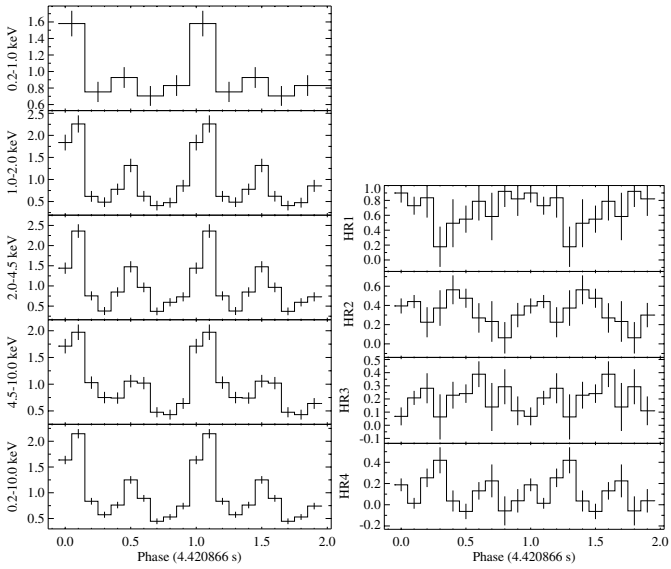

Fig. 6. *Left*: X-ray pulse profile of IGR J05414-6858 in various energy bands from the EPIC-pn time series. The pulse profiles are background-subtracted and normalised to the average net count rate of 3.0, 4.6, 6.8, 8.3 and 22.4 × 10^{-2} cts s^{-1} *from top to bottom*. *Right*: Hardness ratios as a function of pulse phase derived from the pulse profiles in two neighbouring standard energy bands.

3.4. X-ray flux variability

In addition to the fluxes measured in Sect. 3.2, we calculated upper limits for non-detections of IGR J05414-6858. The field was observed by *XMM-Newton* in 2001, but no source was detected by `edetect_chain` (analogous to Sect. 3.1). Spectra were extracted in the same manner as described in Sect. 2 from a 30″ source region and a 50″ background region. Using C statistics and the spectral shape as determined with *XMM-Newton* in 2011, we derived a 90% upper limit for

the flux of 9.0×10^{-14} erg cm^{-2} s^{-1}. This lowest upper limit results in a variability of at least a factor of 100, compared to the maximum flux measured in the *Swift* 2010b observation. Prior to that, we could not find any corresponding X-ray detection. There is no ROSAT source within 1′ listed in the literature.

The *Swift* monitoring of the recent outburst determined the turn-off between MJD 55 786 and 55 793. For the two non-detections, we extracted spectra in the same way as above and determined 90% confidence upper limits of 9.5×10^{-13} erg cm^{-2} s^{-1} and 2.3×10^{-12} erg cm^{-2} s^{-1}. The long-term evolution of the system is presented in Fig. 7.

The variability during the *XMM-Newton* observation in 2011 was at a moderate level. We created a background-corrected light curve, merged using all EPIC instruments and binned to 70 s, corresponding to 30 cts bin^{-1} on average. A χ^2 test of this light curve against a constant resulted in χ^2/d.o.f. = 130/121.

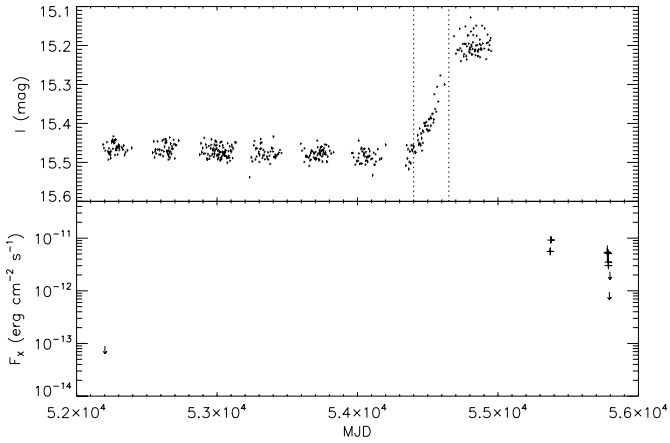

Fig. 7. *I*-band light curve of OGLEIII LMC175.4.21714 (*upper panel*) compared to the X-ray fluxes with upper limits marked by arrows (*lower panel*). Dotted lines separate the optical low, transition, and high state.

4. Analysis and results of optical data

Using GROND, the counterpart of the *Swift* X-ray source was resolved into three point sources. Star A of Rau et al. (2010) was originally classified to be of spectral type B1-2 III from GROND and *Swift*/UVOT photometry and is the most likely counterpart within the improved *XMM-Newton* X-ray position uncertainty of IGR J05414-6858.

The possible northern counterpart at $05^h41^m26\overset{s}{.}57$ −69°01′21″.7 has a somewhat larger angular separation to the X-ray position of 1.3″ (2.6σ). The *I*-band light curve derived from OGLE is flat. GROND photometry (g' = 17.54 ± 0.08, r' = 17.55 ± 0.05, i' = 17.12 ± 0.05, z' = 16.89 ± 0.05, J = 16.49 ± 0.05, H = 16.37 ± 0.05, and K_s = 16.62 ± 0.08) can be modelled by emission from a K star. This is too faint and too red for a Be star. Depending on its luminosity class, the star can be located in the LMC or the Galaxy. In the latter case, coronal X-ray emission would be significantly softer than observed for IGR J05414-6858. Therefore we reject this star as possible optical counterpart in the following. Since there is no soft source detected in the 2001 *XMM-Newton* observation to a limit of 0.005 cts s^{-1}, X-ray emission of this star is unlikely to contribute to the X-ray spectrum of IGR J05414-6858.

4.1. Photometry

The OGLE III *I*-band light curve of this star is presented in Fig. 7. It exhibits two different brightness states with a transition phase in between. Before MJD 54 400 (left dotted line in Fig. 7), the *I*-band emission is at (15.51−15.43) mag, followed by a steep increase to the high state. After MJD 54 650 (right dotted line in Fig. 7), the *I*-band emission is in between (15.24−15.13) mag.

A Lomb-Scargle (Lomb 1976; Scargle 1982) periodogram of the low and high state of the OGLE III light curve is shown in Fig. 8. The high state reveals a periodicity with 19.9 days. The folded light curve of the high state is presented in Fig. 9. Dotted and dashed lines mark the phases of X-ray detections and non detections of 2011, respectively.

The *Swift*/UVOT photometry is presented in Table 3. Within uncertainties most values are constant. For the 2010 measurements, we see an indication for a flux decrease in the *uvm*2 and *uvw*2 magnitudes of ∼0.13 ± 0.04 mag and ∼0.17 ± 0.04 mag, respectively. Other magnitudes in 2011 are constant, except for a possible short increase in the UV on 2011-08-13 between 22:49 and 23:12 by ∼0.1 mag. These are of the same order as the variations observed by OGLE during high and low state.

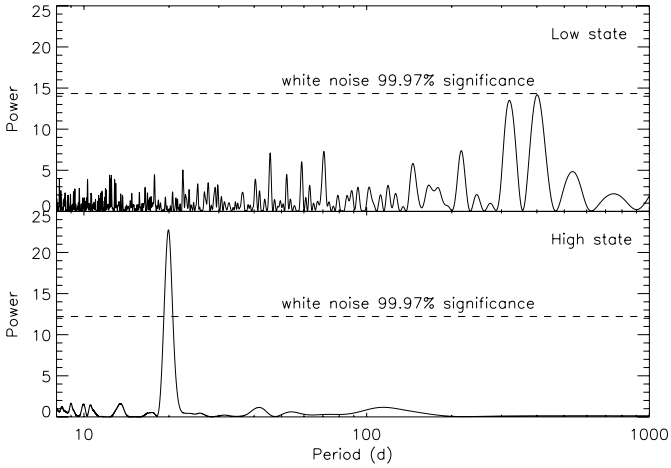

Fig. 8. Lomb-Scargle periodogram of the *I*-band of OGLEIII LMC175.4.21714 for the low state (*upper panel*) and high state (*lower panel*).

By comparing the averaged magnitudes of 2010-06-25 and those of 2011, we find a stronger flux increase as observed with OGLE III in 2008, with Δv = −0.36 mag, Δb = −0.30 mag, Δu = −0.31 mag, $\Delta uvw1$ = −0.20 mag, $\Delta uvm2$ = −0.20 mag, and $\Delta uvw2$ = −0.18 mag. This indicates yet another transition from low to high state between June 2010 and August 2011.

The GROND magnitudes are summarised in Table 4. Owing to pointing constraints, the first observation was performed only in the J, H, and K_s bands, while the remaining epochs cover all seven channels. Note the increase in magnitude between 2010-06-26 and 2010-06-29 of ΔJ = (0.25 ± 0.07) mag, ΔH = (0.45 ± 0.07) mag, and ΔK_s = (0.42 ± 0.11) mag within three days. This affirms the observed drop of the flux as observed with *Swift*/UVOT.

The fit to the spectral energy distribution composed from the first GROND epoch together with averaged UVOT photometry from 2010 June 25 is shown in Fig. 10. Here, all magnitudes were corrected for Galactic reddening of E_{B-V} = 0.075 mag (Schlegel et al. 1998) using the Cardelli et al. (1989) extinction law and for the LMC-intrinsic reddening of E_{B-V} = 0.15 mag (see Sect. 4.2) using the Pei (1992) extinction law. The data are best fitted with a hot (≈31 000 K) black-body spectrum, consistent with the B0-1 III stellar classification suggested by

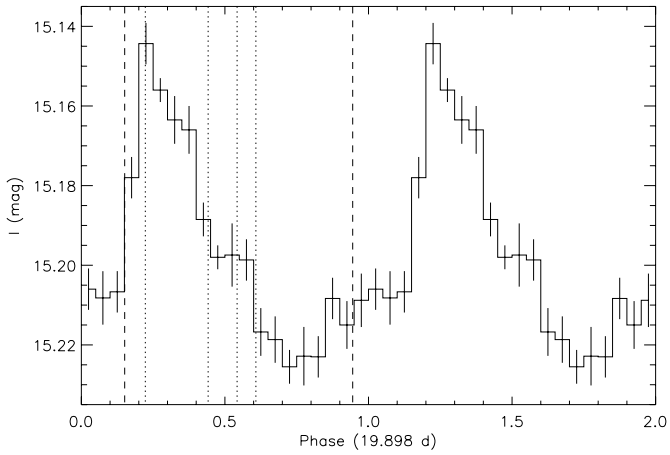

Fig. 9. *I*-band light curve from OGLE III in the high state convolved with 19.898 days. Phase = 0 corresponds to MJD 54 640. Dotted lines give the phase of the beginning of the X-ray observations in 2011. Dashed lines mark the *Swift*/XRT non-detections.

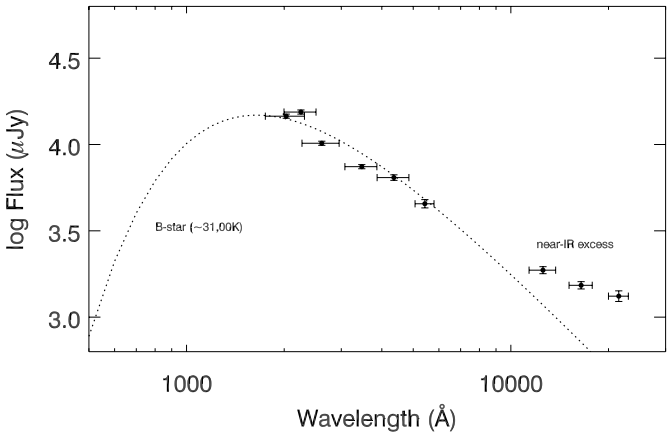

Fig. 10. UV-near-IR SED composed of *Swift*/UVOT observations obtained on 2010 June 25 and GROND data taken on 2010 June 26. The dotted line shows the simplified best-fit black-body model, indicating that the UVOT photometry is consistent with the B0-1 stellar classification derived from the spectroscopy.

the optical spectroscopy (Sect. 4.2). We note that there is a clear excess in the near-IR bands.

4.2. Spectral classification

OB stars in our own Galaxy are classified using the ratio of certain metal and helium lines (Walborn & Fitzpatrick 1990) based on the Morgan-Keenan (MK; Morgan et al. 1943) system. However, this is unsuitable in lower metallicity environments because the metal lines are either much weaker or not present. As such, the optical spectrum of IGR J05414-6858 was classified using the method developed by Lennon (1997) for B-type stars in the SMC and implemented for the SMC, LMC and Galaxy by (Evans et al. 2004, 2006). This system is normalised to the MK system such that stars in both systems show the same trends in their line strengths. The luminosity classification method from Walborn & Fitzpatrick (1990) was assumed in this work.

Figure 11 shows the unsmoothed optical spectrum of IGR J04514-6858. The spectrum is dominated by the hydrogen Balmer series and neutral helium lines. The He I line at λ4143 Å is stronger than the He II λ4200 Å, which means the star is later than type O9. He II λ4686 Å is also clearly present, implying that the optical counterpart of IGR J04514-6858 is earlier than type B1.5, although the He II λ4541 Å line is not

Table 3. *Swift*/UVOT photometry.

Filter	UT date	AB Mag[a]
v	2010-06-25 06:09	15.47 ± 0.06
	07:51	15.51 ± 0.06
	2011-08-10 00:36	15.11 ± 0.04
	02:15	15.20 ± 0.05
	03:53	15.10 ± 0.05
	2011-08-13 23:07	15.13 ± 0.04
b	2010-06-25 06:02	15.36 ± 0.04
	07:45	15.43 ± 0.04
	09:28	15.34 ± 0.04
	2011-08-10 00:24	15.08 ± 0.03
	02:06	15.08 ± 0.03
	03:48	15.07 ± 0.04
	2011-08-13 22:55	15.07 ± 0.03
	2011-08-20 17:13	15.10 ± 0.03
u	2010-06-25 06:00	15.41 ± 0.03
	07:43	15.38 ± 0.03
	09:26	15.35 ± 0.03
	2011-08-10 00:21	15.06 ± 0.03
	02:05	15.04 ± 0.03
	03:46	15.05 ± 0.03
	05:17	15.05 ± 0.05
	2011-08-13 22:52	15.10 ± 0.03
	2011-08-20 17:11	15.12 ± 0.03
uvw1	2010-06-25 05:58	15.45 ± 0.03
	07:41	15.44 ± 0.03
	09:24	15.44 ± 0.03
	2011-08-10 00:17	15.20 ± 0.03
	02:02	15.25 ± 0.03
	03:45	15.24 ± 0.03
	05:15	15.26 ± 0.03
	2011-08-13 22:49	15.31 ± 0.03
	2011-08-20 17:08	15.22 ± 0.03
uvm2	2010-06-25 06:19	15.56 ± 0.02
	07:59	15.57 ± 0.03
	2010-07-01 00:13	15.70 ± 0.03
	2011-08-10 00:41	15.29 ± 0.03
	02:18	15.41 ± 0.03
	03:55	15.38 ± 0.03
	2011-08-13 00:31	15.33 ± 0.03
	02:06	15.33 ± 0.02
	23:12	15.43 ± 0.03
uvw2	2010-06-25 06:05	15.60 ± 0.03
	07:48	15.63 ± 0.03
	09:30	15.61 ± 0.03
	2010-06-30 01:40	15.59 ± 0.02
	03:21	15.97 ± 0.02
	04:49	15.61 ± 0.02
	17:56	15.71 ± 0.02
	19:32	15.70 ± 0.02
	22:35	15.77 ± 0.03
	2011-08-10 00:30	15.36 ± 0.02
	02:11	15.48 ± 0.02
	03:50	15.42 ± 0.03
	2011-08-13 23:01	15.54 ± 0.02
	2011-08-20 01:00	15.41 ± 0.02
	17:15	15.38 ± 0.04
	2011-08-24 03:10	15.44 ± 0.02
	04:46	15.45 ± 0.02

Notes. [(a)] Not corrected for Galactic foreground reddening or extinction in the LMC.

Table 4. GROND photometry.

UT date	AB magnitude[a]						
	g'	r'	i'	z'	J	H	K_s
2010-06-26 10:51	–	–	–	–	15.93 ± 0.05	16.07 ± 0.05	16.29 ± 0.07
2010-06-29 10:29	15.34 ± 0.04	15.60 ± 0.03	15.82 ± 0.03	15.98 ± 0.04	16.17 ± 0.05	16.53 ± 0.05	16.71 ± 0.08
2012-01-25 04:14	15.18 ± 0.04	15.41 ± 0.03	15.57 ± 0.03	15.72 ± 0.04	15.96 ± 0.05	16.28 ± 0.05	16.54 ± 0.08

Notes. [(a)] Not corrected for Galactic foreground reddening or extinction in the LMC.

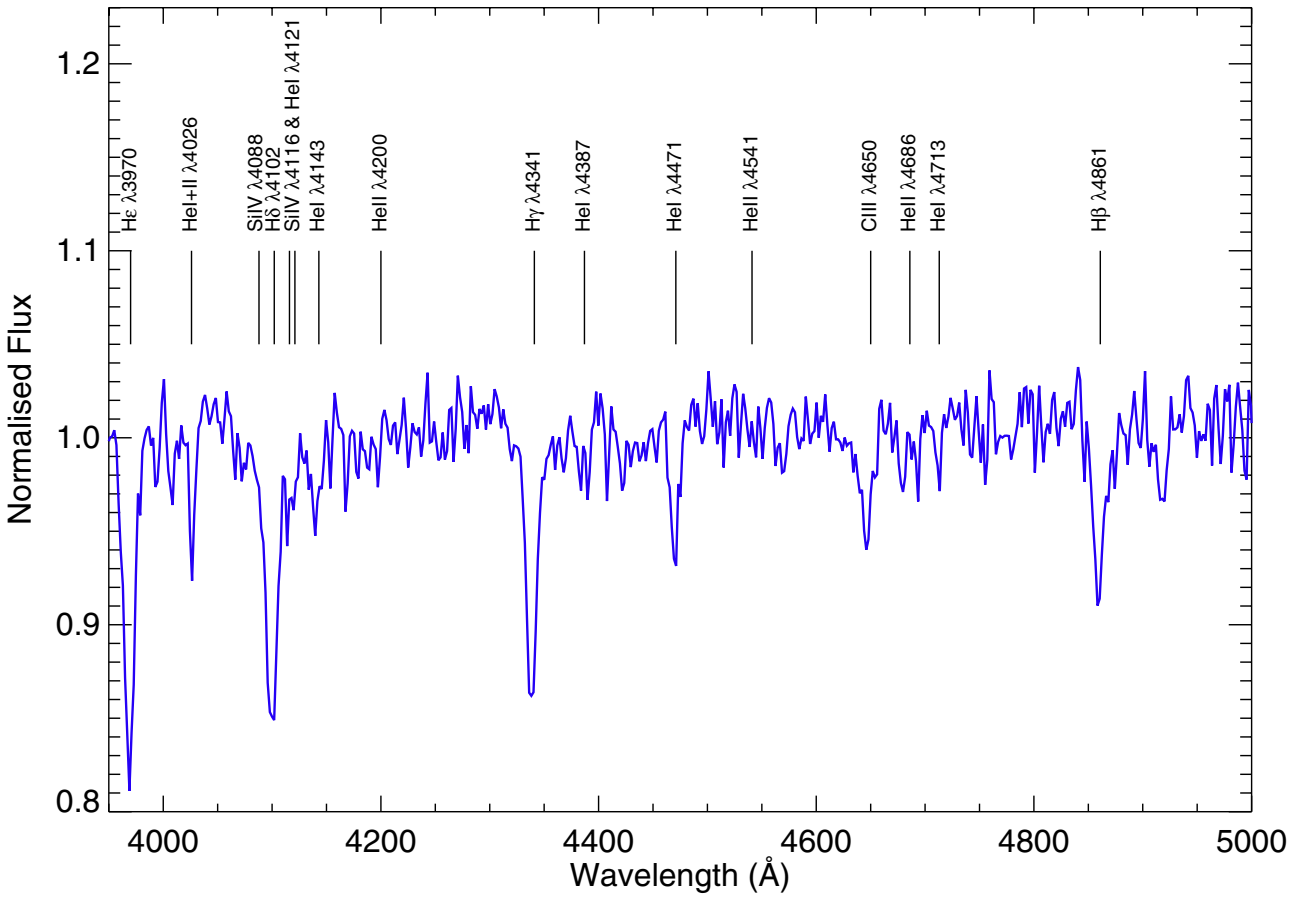

Fig. 11. Spectrum of IGR J04514-6858 in the wavelength range $\lambda\lambda$3900−5000 Å with the NTT on 2011-12-08. The spectrum has been normalised to remove the continuum and was redshift-corrected by −280 km s^{-1}. Atomic transitions relevant to spectral classification have been marked.

visible above the noise level of the data. There is also evidence for the Si IV λ4116 Å line – consistent with a spectral classification of B1. However, Walborn & Fitzpatrick (1990) present spectra of B0 type stars with clear Si lines, indicating that a spectral classification of B0 is not ruled out by their presence. We note that there does not appear to be any evidence for the Si IV λ4088 Å line. Be stars are characterised by their rapid rotation velocity and it could be that this line is concealed by the rotationally broadened Hδ line in close proximity.

The luminosity class of the system was determined using the ratios of S IV λ4116/He I λ4121, He I λ4121/He I λ4143 and He II λ4686/He I λ4713. The first two ratios increase with decreasing luminosity class (i.e. with increasing luminosity), whereas the latter ratio decreases with increasing luminosity. The relative strengths of these lines suggest a luminosity class III, making our spectral classification of B0-1 III consistent with that obtained photometrically with the GROND and *Swift*/UVOT data. To check the spectral identification we can compare the observed optical magnitudes with that predicted for a B0-1 III star in the LMC. Taking the faintest, least disc-contaminated V-band magnitude from Table 3 of V = (15.51 ± 0.06) mag, a distance modulus of 18.5 ± 0.1 (Koerwer 2009) and a reddening of E_{B-V} = 0.15 mag (Schwering & Israel 1991) reveals an absolute magnitude for the star of M_V = (−3.5 ± 0.2). This value would be consistent with a B0.5 III star (Wegner 2006) and hence confirms the classification deduced from the spectra reported here. We note that we cannot use the derived X-ray absorption reported here to refine the column to the star because of the large uncertainties in that value.

Figure 12 shows the red end of the spectrum of IGR J04514-6858 taken near-simultaneously. The Hα equivalent width, considered an indicator for circumstellar disc size, is relatively small at −(3.2 ± 0.6) Å which is consistent with the lack of Hβ in emission in Fig. 11. The double peaked, asymmetric nature of the line profile shows a V/R pattern consistent with global one armed oscillations (GOAO) and suggests that the circumstellar disc of the star is inclined to the line of sight. This is not uncommon in the circumstellar discs of Be stars.

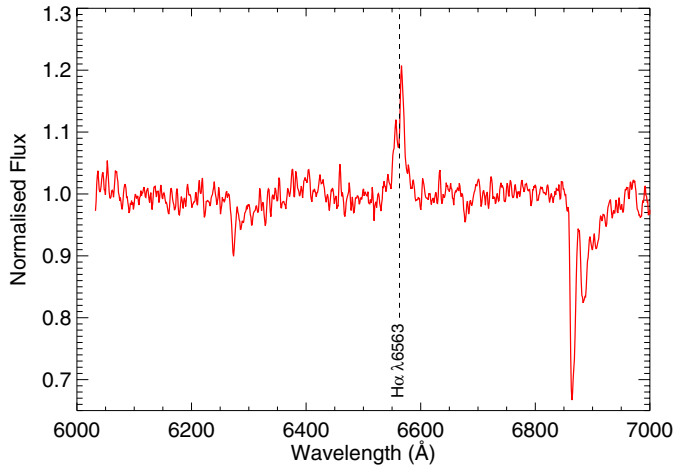

Fig. 12. Spectrum of IGR J04514-6858 in the wavelength range $\lambda\lambda$6000−7000 Å with the NTT on 2011-12-10. The spectrum has been smoothed with a boxcar average of 3, normalised to remove the continuum and shifted by −280 km s^{-1}.

5. Discussion and conclusions

We performed an *XMM-Newton* ToO observation of IGR J05414-6858 in August 2011, allowing us to measure the X-ray spectrum and discover the spin period. This adds the tenth known HMXB pulsar to the LMC sample and confirms the neutron star nature of the compact object.

The source was found in INTEGRAL observations performed on 2010 May 13−22 (130 ks) and June 6−14 (400 ks) at an average flux of 8×10^{36} erg s^{-1} in the (20−40) keV band (Grebenev & Lutovinov 2010). In the *Swift* follow-up observation on June 30 we see the source still in outburst at a luminosity of $\sim 3 \times 10^{36}$ erg s^{-1} in the (0.2−10.0) keV band. If these detections correspond to the same outburst, the duration of X-ray bright state would suggest a type-II outburst. The luminosity, derived from INTEGRAL is at the lower limit for a classical type-II outburst, but might have been higher at maximum. The luminosity and observed duration of the 2011 outburst agree with a type-I outburst, but since the time of the beginning of the outburst is unknown, we cannot exclude a type-II outburst.

Furthermore, the spectrum of the current outburst was found to be significantly harder than in 2010. The power-law photon index of the 2011 outburst of $\Gamma = 0.3-0.4$ is also relatively low, compared to the distribution known from the SMC sample ($\Gamma \sim 1$). We note that for a few BeXRBs in the SMC hard spectra were also observed, e.g. for the pulsars XTE J0103-728 ($\Gamma = 0.35-0.54$, $P_{\rm spin} = 6.85$ s, Haberl & Pietsch 2008) and XMMU J004814.0-732204 ($\Gamma = 0.53-0.66$, $P_{\rm spin} = 11.87$ s, Sturm et al. 2011a). The first one of these also was detected in a type-II outburst with INTEGRAL (Townsend et al. 2010). Moreover, for both SMC pulsars an indication of a soft excess with comparable emission radius was found and was suggested to originate from the accretion disc. The system intrinsic absorption strongly depends on the modelling ($0-5 \times 10^{21}$ cm^{-2}) and the location of the system in the LMC. The total LMC column density along the line of sight at the position of IGR J05414-6858 is 3.6×10^{21} cm^{-2} (Kim et al. 2003).

According to the Corbet relation (Corbet 1984; Laycock et al. 2005; Corbet et al. 2009), we expect the orbital period of the system in the range of (1−100) days for the measured spin period of IGR J05414-6858. The periodic variations seen in the *I*-band are therefore likely caused by binarity. Assuming masses of 21.5 $M_\odot$ and 1 $M_\odot$ for the Be star and the NS, respectively, the orbital period implies a semi-major axis of the binary system of 0.41 AU, corresponding to ∼6 stellar radii (Vacca et al. 1996). The X-ray detections in 2011 occurred during the bright phase of the folded *I*-band light curve (see dotted lines in Fig. 9). In 2011, the X-ray luminosity follows the *I*-band emission and the non-detections were during low *I*-band emission. A correlation of X-ray and optical outbursts was e.g. reported for AX J0058-720 (Haberl & Pietsch 2007). In the case of the 2010 outburst, the two *Swift* X-ray detections are during low *I*-band emission at phase 0.80 and 0.04. This is either because type-II outbursts are not correlated to the orbital phase, or because the optical period is not caused by binarity.

Long-term optical variation with different variability patterns are typical for BeXRBs (Rajoelimanana et al. 2011). An explanation for the transition from low to high state by $\Delta I \sim 0.3$ mag might be the build-up of a decretion disc around the Be star. The *XMM-Newton* upper limit (X-ray faint state) in 2001 was during the optical low state, where there probably was no decretion disc. From other BeXRBs (cf. Fig. 10 of Reig 2011), a correlation between NIR and optical magnitudes is seen. Therefore it is likely that the long-term variability seen in the OGLE *I*-band extends from NIR to UV. As indicated by the GROND and *Swift*/UVOT observations, the system still undergoes strong variations in the NIR, optical, and UV. A rapid strong drop in the NIR emission was observed between June 2010 26th and 29th. At this time, the source was still in a presumable type-II X-ray outburst, which can be followed by a disc loss phase. The NIR-flux decrease additionally supports a type-II outburst. Also, the $K_{\rm s}$-band magnitude was high, compared to the GROND January 2012 observation, while *J* was at the same level, again pointing to the presence of a circumstellar disc. This is also supported by the Hα line emission in December 2011. Unfortunately, the end of the 2010 X-ray outburst is not constrained. During the 2011 outburst, the *Swift*/UVOT observations do not indicate any strong changes in the optical. Forthcoming OGLE IV data will allow us to extend the light curve and to confirm the periodicity.

IGR J05414-6858 is the tenth known HMXB pulsar in the LMC with $P_{\rm spin} = 4.4208$ s. The optical counterpart was classified to be of spectral type B0-1 IIIe and shows double-peaked Hα emission and a variable NIR excess. A likely orbital period of $P_{\rm orb} = 19.9$ d was found. The two observed X-ray outbursts demonstrate the importance of optical monitoring during outbursts, to better understand the accretion process in these systems. To increase the sample of explored HMXB in the LMC even more, further X-ray observations triggered during an outburst are necessary.

Acknowledgements. We thank the *XMM-Newton* team for scheduling the ToO observation. The *XMM-Newton* project is supported by the Bundesministerium für Wirtschaft und Technologie/Deutsches Zentrum für Luft- und Raumfahrt (BMWI/DLR, FKZ 50 OX 0001) and the Max-Planck Society. Part of the funding for GROND (both hardware as well as personnel) was generously granted from the Leibniz-Prize to Prof. G. Hasinger (DFG grant HA 1850/28-1). The OGLE project has received funding from the European Research Council under the European Community's Seventh Framework Programme (FP7/2007−2013)/ERC grant agreement No. 246678 to AU. We acknowledge the use of public data from the *Swift* data archive. X.-LZ. acknowledges financial support by DLR FKZ 50 OG 0502. R.S. acknowledges support from the BMWI/DLR grant FKZ 50 OR 0907.

References

Antoniou, V., Zezas, A., Hatzidimitriou, D., & Kalogera, V. 2010, ApJ, 716, L140

Arnaud, K. A. 1996, in Astronomical Data Analysis Software and Systems V, ed. G. H. Jacoby, & J. Barnes, ASP Conf. Ser., 101, 17

Buccheri, R., Bennett, K., Bignami, G. F., et al. 1983, A&A, 128, 245
Cardelli, J. A., Clayton, G. C., & Mathis, J. S. 1989, ApJ, 345, 245
Coe, M. J. 2005, MNRAS, 358, 1379
Coe, M., Corbets, R. H. D., McGowan, K. E., & McBride, V. A. 2010, in High Energy Phenomena in Massive Stars, ed. J. Martí, P. L. Luque-Escamilla, & J. A. Combi, ASP Conf. Ser., 422, 224
Corbet, R. H. D. 1984, A&A, 141, 91
Corbet, R. H. D., Coe, M. J., McGowan, K. E., et al. 2009, in IAU Symp. 256, ed. J. T. van Loon, & J. M. Oliveira, 361
Dickey, J. M., & Lockman, F. J. 1990, ARA&A, 28, 215
Eger, P., & Haberl, F. 2008, A&A, 491, 841
Evans, C. J., Howarth, I. D., Irwin, M. J., Burnley , A. W., & Harries, T. J. 2004, MNRAS, 353, 601
Evans, C. J., Lennon, D. J., Smartt, S. J., & Trundle, C. 2006, A&A, 456, 623
Galache, J. L., Corbet, R. H. D., Coe, M. J., et al. 2008, ApJS, 177, 189
Grebenev, S. A., & Lutovinov, A. A. 2010, The Astronomer's Telegram, 2695, 1
Gregory, P. C., & Loredo, T. J. 1996, ApJ, 473, 1059
Greiner, J., Bornemann, W., Clemens, C., et al. 2008, PASP, 120, 405
Haberl, F., & Pietsch, W. 2007, A&A, 476, 317
Haberl, F., & Pietsch, W. 2008, A&A, 484, 451
Haberl, F., & Zavlin, V. E. 2002, A&A, 391, 571
Haberl, F., Eger, P., & Pietsch, W. 2008, A&A, 489, 327
Hickox, R. C., Narayan, R., & Kallman, T. R. 2004, ApJ, 614, 881
Jansen, F., Lumb, D., Altieri, B., et al. 2001, A&A, 365, L1
Kim, S., Staveley-Smith, L., Dopita, M. A., et al. 2003, ApJS, 148, 473
Knigge, C., Coe, M. J., & Podsiadlowski, P. 2011, Nature, 479, 372
Koerwer, J. F. 2009, AJ, 138, 1
Krühler, T., Küpcü Yoldaş, A., Greiner, J., et al. 2008, ApJ, 685, 376
Laycock, S., Corbet, R. H. D., Coe, M. J., et al. 2005, ApJS, 161, 96
Lennon, D. J. 1997, A&A, 317, 871
Lomb, N. R. 1976, Ap&SS, 39, 447
Lutovinov, A., & Grebenev, S. 2010, The Astronomer's Telegram, 2696, 1
Mineo, S., Gilfanov, M., & Sunyaev, R. 2011, Astron. Nachr., 332, 349
Morgan, W. W., Keenan, P. C., & Kellman, E. 1943, An atlas of stellar spectra, with an outline of spectral classification, ed. W. W. Morgan, P. C. Keenan, & E. Kellman
Okazaki, A. T. 2001, PASJ, 53, 119
Paturel, G., Dubois, P., Petit, C., & Woelfel, F. 2002, LEDA, 0
Pei, Y. C. 1992, ApJ, 395, 130
Poole, T. S., Breeveld, A. A., Page, M. J., et al. 2008, MNRAS, 383, 627
Rajoelimanana, A. F., Charles, P. A., & Udalski, A. 2011, MNRAS, 413, 1600
Rau, A., Schady, P., Greiner, J., Haberl, F., & Updike, A. 2010, The Astronomer's Telegram, 2704, 1
Reig, P. 2011, Ap&SS, 332, 1
Russell, S. C., & Dopita, M. A. 1992, ApJ, 384, 508
Scargle, J. D. 1982, ApJ, 263, 835
Schlegel, D. J., Finkbeiner, D. P., & Davis, M. 1998, ApJ, 500, 525
Schwering, P. B. W., & Israel, F. P. 1991, A&A, 246, 231
Skrutskie, M. F., Cutri, R. M., Stiening, R., et al. 2006, AJ, 131, 1163
Strüder, L., Briel, U., Dennerl, K., et al. 2001, A&A, 365, L18
Sturm, R., Haberl, F., Coe, M. J., et al. 2011a, A&A, 527, A131
Sturm, R., Haberl, F., Pietsch, W., & Immler, S. 2011b, The Astronomer's Telegram, 3537, 1
Townsend, L. J., Coe, M. J., McBride, V. A., et al. 2010, MNRAS, 403, 1239
Turner, M. J. L., Abbey, A., Arnaud, M., et al. 2001, A&A, 365, L27
Udalski, A., Szymanski, M. K., Soszynski, I., & Poleski, R. 2008, Acta Astron., 58, 69
Vacca, W. D., Garmany, C. D., & Shull, J. M. 1996, ApJ, 460, 914
Walborn, N. R., & Fitzpatrick, E. L. 1990, PASP, 102, 379
Wegner, W. 2006, MNRAS, 371, 185
Wilms, J., Allen, A., & McCray, R. 2000, ApJ, 542, 914